NiO addition effects on Ba(Zr, Ce, Y)$O_{3-\delta}$: sintering behavior and proton uptake

Yuanye Huang [1,#], Rotraut Merkle [1], Joachim Maier [1]

[1] Max Planck Institute for Solid State Research, Heisenbergstraße 1, Stuttgart, 70569, Germany

[#] present address: Empa, Swiss Federal Laboratories for Materials Science and Technology, Überlandstraße 129, 8600, Dübendorf, Switzerland

Supplementary Information

Table S1: Composition of pellets sintered by SSRS, and SPS with Ni on B site. SSRS samples were sintered at 1550 ˚C 4 h. SPS samples were sintered at 1350 ˚C and 1300 ˚C for 1 at% and 4 at% Ni and annealed at 1400 ˚C 4 h.

Nominal Composition	Measurement by ICP-OES / wt.%					Real composition	A: B ratio
	Ba	Zr	Ce	Y	Ni		
BZC20Y13.6-0.125Ni	48.5 ±0.5	20.7 ±0.3	9.61 ±0.1	4.12 ±0.05	0.126 ±0.009	$Ba_{1.02}Zr_{0.66}Ce_{0.20}Y_{0.13}Hf_{0.01}O_{3-\delta}$ + 0.16 wt.% NiO	1.02
BZC20Y13.6-0.25Ni	48.4 ±0.5	20.5 ±0.3	9.69 ±0.1	4.11 ±0.05	0.163 ±0.01	$Ba_{1.03}Zr_{0.66}Ce_{0.20}Y_{0.13}Hf_{0.01}O_{3-\delta}$ + 0.21 wt.% NiO	1.03
BZC20Y13.6-0.375Ni	48.2 ±0.5	21.5 ±0.3	9.02 ±0.1	4.59 ±0.06	0.344 ±0.01	$Ba_{0.99}Zr_{0.67}Ce_{0.18}Y_{0.15}Hf_{0.01}O_{3-\delta}$ + 0.44 wt.% NiO	0.99
BZC20Y13.6-0.5Ni	48.2 ±0.5	20.6 ±0.3	9.55 ±0.1	4.01 ±0.09	0.35 ±0.03	$Ba_{1.03}Zr_{0.66}Ce_{0.20}Y_{0.13}Hf_{0.01}O_{3-\delta}$ + 0.45 wt.% NiO	1.03
BZC20Y13.6-1.0Ni	48.2 ±0.5	20.7 ±0.3	9.78 ±0.1	4.01 ±0.05	0.41 ±0.03	$Ba_{1.01}Zr_{0.66}Ce_{0.20}Y_{0.13}Hf_{0.01}O_{3-\delta}$ + 0.52 wt.% NiO	1.02
BZC20Y13.6Ni1-SPS	48.0 ±0.5	20.6 ±0.3	9.85 ±0.1	4.56 ±0.09	0.25 ±0.01	$Ba_{0.99}Zr_{0.64}Ce_{0.20}Y_{0.14}Ni_{0.01}Hf_{0.01}O_{3-\delta}$	0.99
BZC20Y13.6Ni4-SPS	47.8 ±0.5	20.1 ±0.3	9.88 ±0.1	4.47 ±0.09	0.56 ±0.04	$Ba_{0.99}Zr_{0.62}Ce_{0.20}Y_{0.14}Ni_{0.03}Hf_{0.01}O_{3-\delta}$	0.99

Table S2: Composition of BZCY with 1.0 wt% NiO addition sintered at 1550 ˚C for different time.

Sintering time / h	Measurement by ICP-OES / wt.%					Real composition	A: B ratio
	Ba	Zr	Ce	Y	Ni		
1	48.2 ±0.5	21.6 ±0.3	9.68 ±0.1	4.19 ±0.06	0.487 ±0.005	$Ba_{0.99}Zr_{0.67}Ce_{0.19}Y_{0.13}Hf_{0.01}O_{3-\delta}$ + 0.62 wt.% NiO	0.99
4	48.2 ±0.5	20.7 ±0.3	9.78 ±0.1	4.01 ±0.05	0.41 ±0.03	$Ba_{1.02}Zr_{0.66}Ce_{0.20}Y_{0.13}Hf_{0.01}O_{3-\delta}$ + 0.52 wt.% NiO	1.02
16	48.1 ±0.5	20.8 ±0.3	9.67 ±0.1	4.19 ±0.17	0.377 ±0.007	$Ba_{1.01}Zr_{0.66}Ce_{0.20}Y_{0.14}Hf_{0.01}O_{3-\delta}$ + 0.48 wt.% NiO	1.01

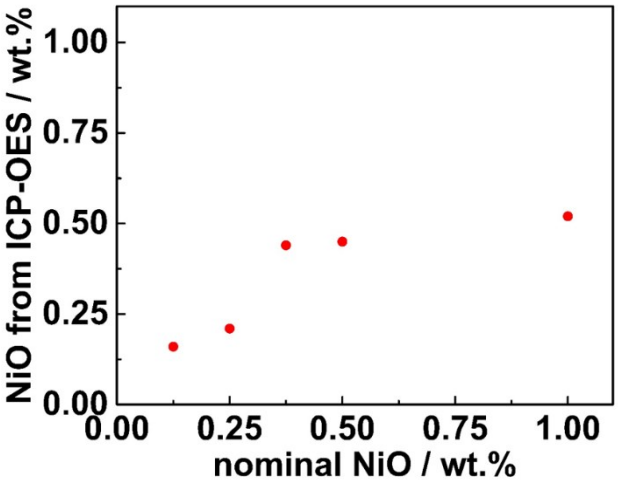

Figure S1: Actual NiO content of SSRS samples sintered at 1550 ˚C 4h from ICP-OES.

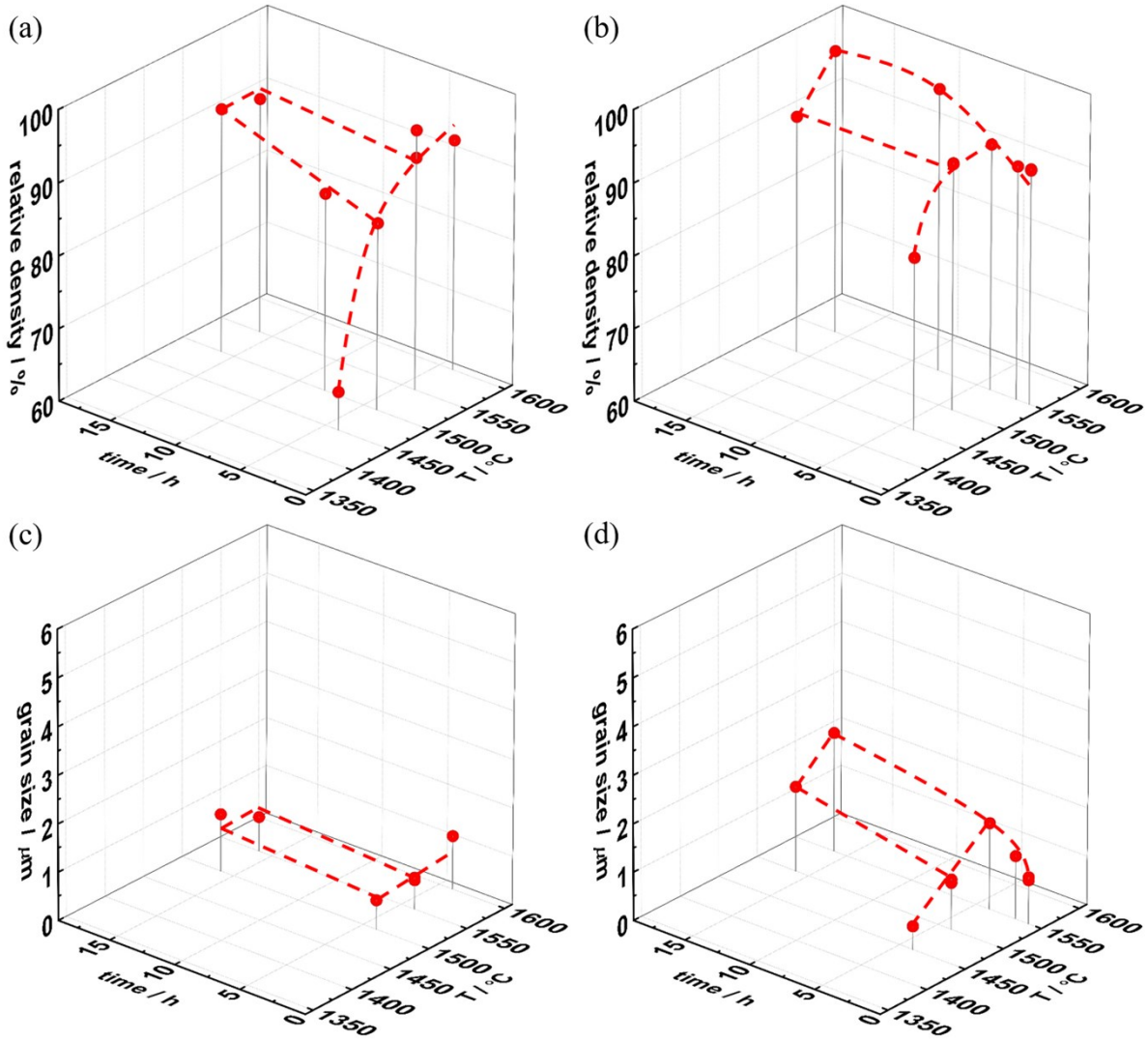

Figure S2: Relative density (top) and grain size (bottom) as function of sintering temperature and soaking time with (a,c) 0.125 wt% NiO, and (b,d) 0.375 wt% NiO. The dashed lines are only a guide to the eye.

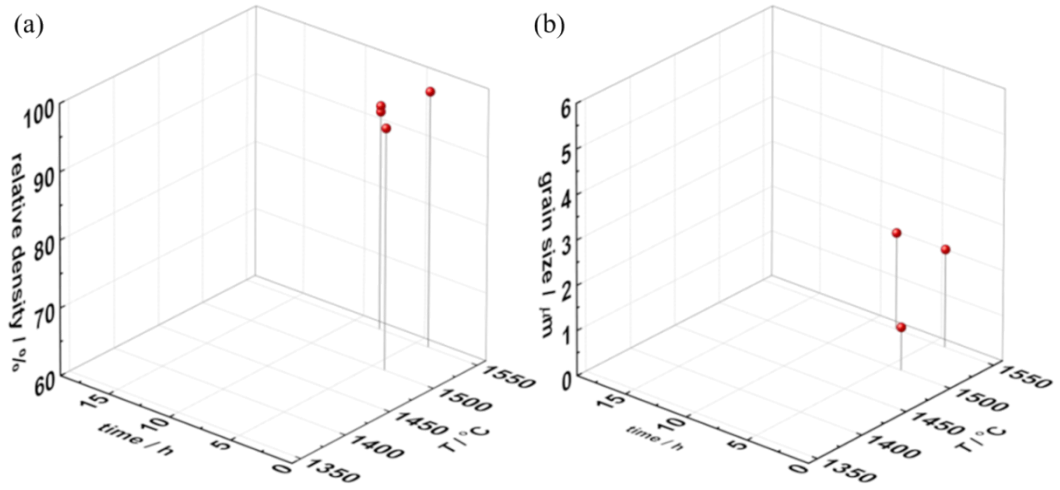

Figure S3: (a) relative density and (b) grain size as function of sintering temperature and soaking time for sample doped with 17.5 at% Y and 0.5 wt% NiO addition.

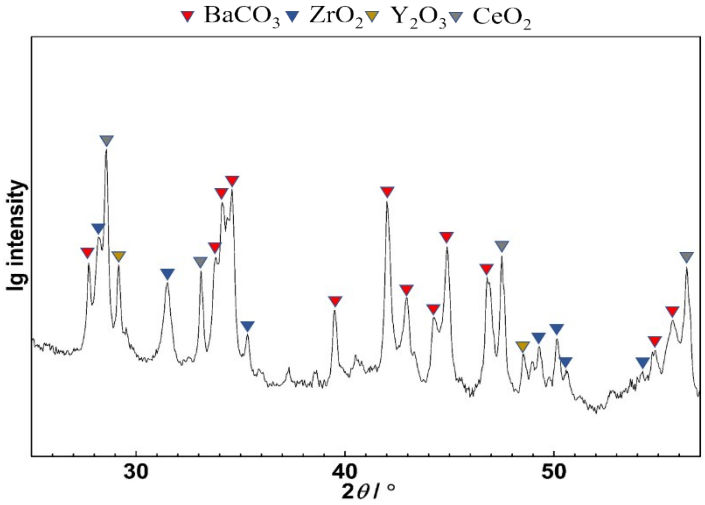

Figure S4: XRD pattern of the wet ball milled powder from the sample with 2.0 wt% NiO addition.

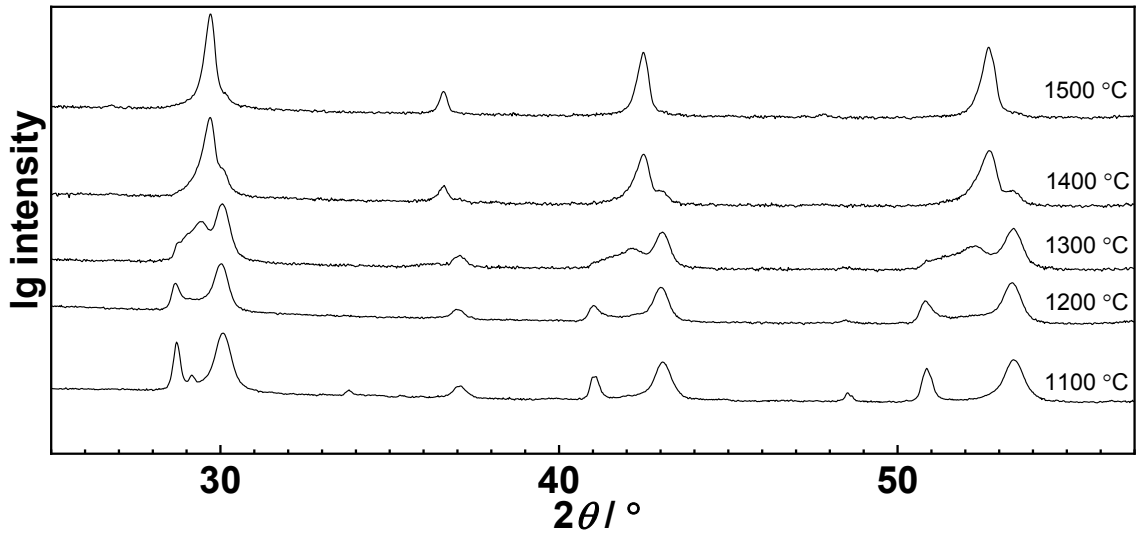

Figure S5: XRD patterns of BZCY with 0.5 wt% NiO addition sintered at different *T* for 10 min.

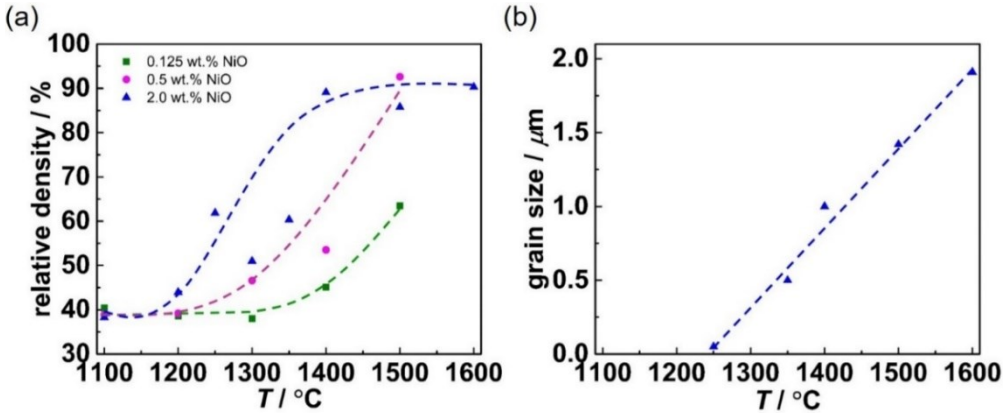

Figure S6: Evolution of grain size and density with temperature for the quenched samples of Fig. 6-7.

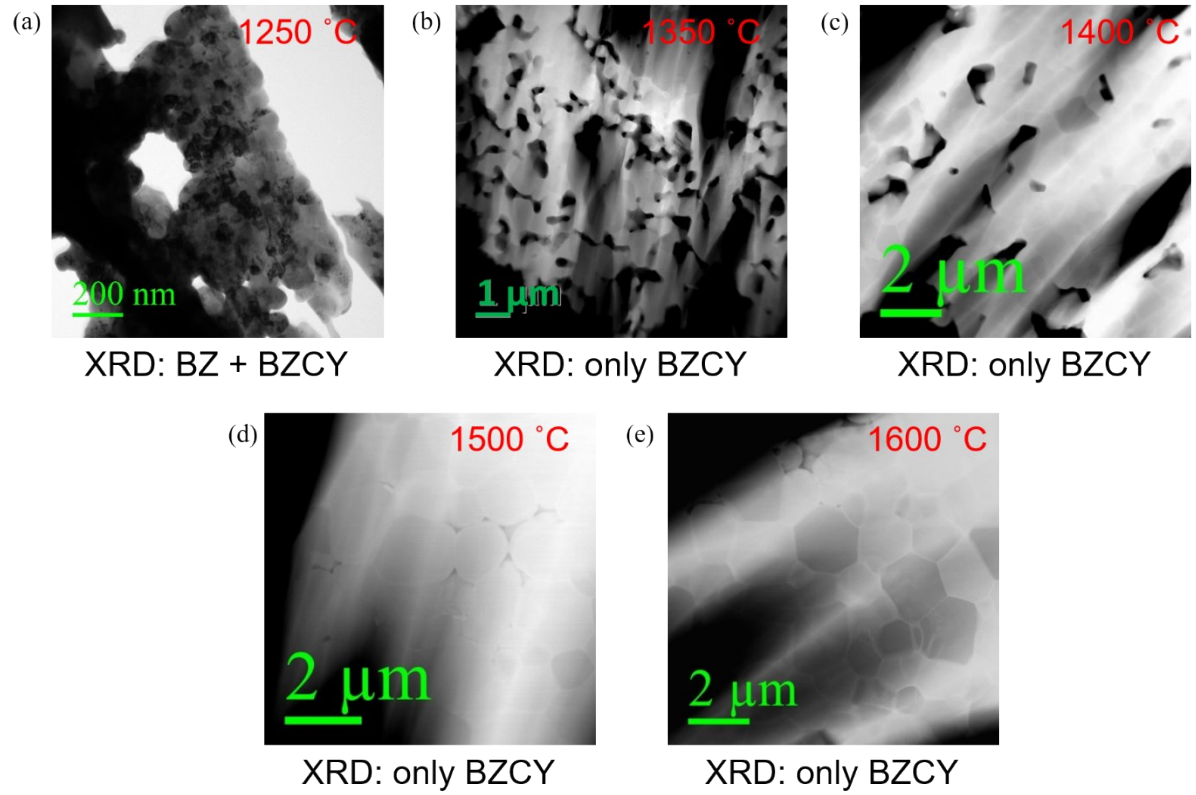

Figure S7: (a) BF image from 1250 ˚C and (b-e) HAADF images from quenched BZCY with 2.0 wt% NiO addition samples sintered for 10 min at different temperatures.

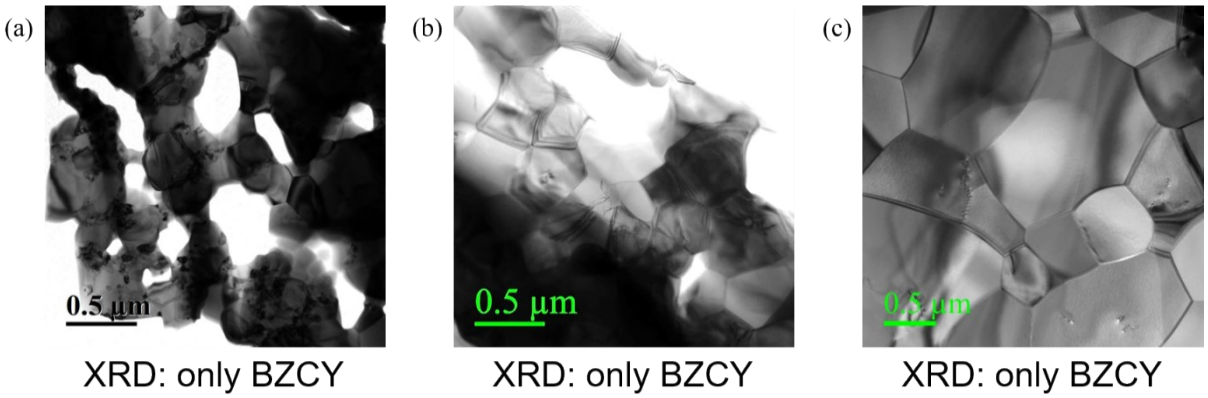

Figure S8: BF images from quenched quenched BZCY with 2.0 wt% NiO addition samples sintered at 1350 ˚C for (a) 10 min, (b) 30 min and (c) 4 h.

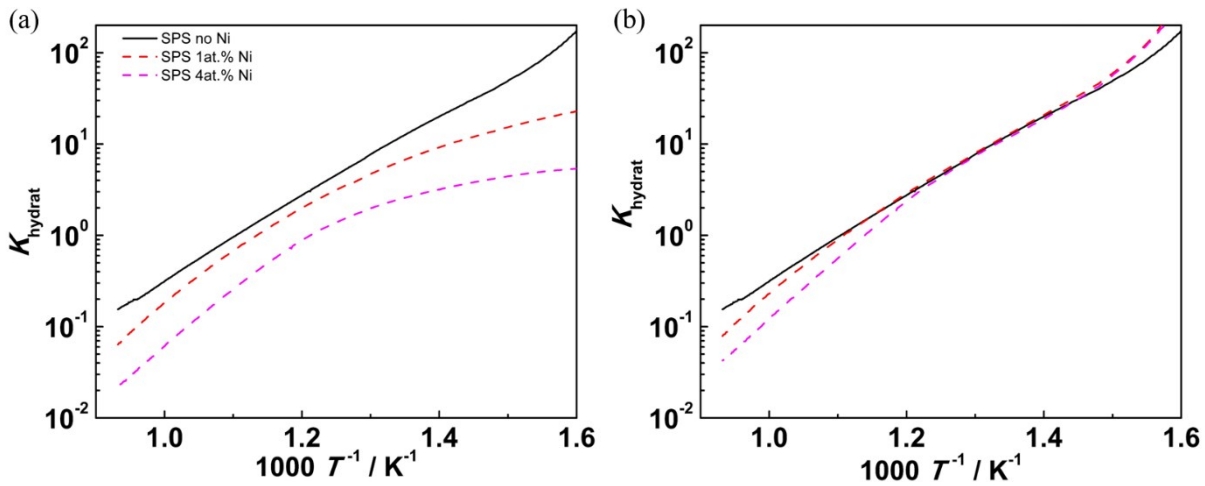

Figure S9: Van't Hoff plots for Ni-free and substitutional-Ni samples, (a) K_{hydrat} calculated with nominal acceptor concentration. (b) Calculated with effective acceptor concentration.

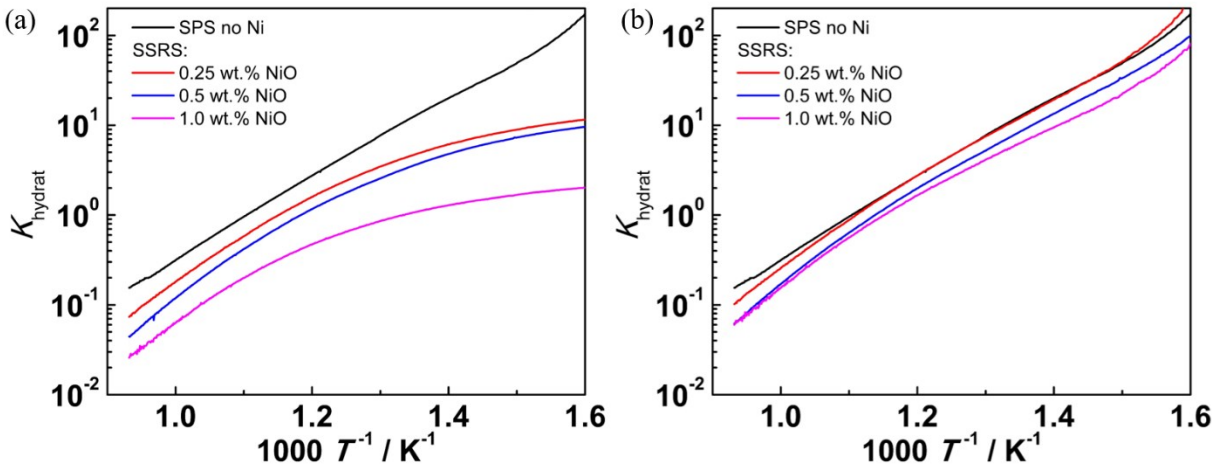

Figure S10: Van't Hoff plots with effective dopant concentration for different excess NiO addition. (a) K_{hydrat} calculated with nominal acceptor concentration. (b) Calculated with effctive acceptor concentration; the linear fitting temperature range for ΔH^o and ΔS^o is 350 – 800 ˚C.

Note that for the Ni-excess samples in Fig. S10a the bending starts already at much higher temperatures (below ≈ 570 °C) compared to the samples with substitutional Ni in Fig. S9a (only below ≈ 420 °C). The stronger bending corresponds to lower effective acceptor concentrations, cf. Fig. 10c in the main paper.

Procedure for [A'$_{eff}$] determination: The plateau which the proton uptake approaches at 300°C (Fig. 10a,b) gives already a rough estimate of [A'$_{eff}$] (when the proton concentration approaches saturation, [$^{OH}_{O}$] = [A'$_{eff}$] holds). The actual [A'$_{eff}$] values of Fig. 10c were determined from this first estimate and the condition that the van 't Hoff plot should become as straight as possible. The use of a modified electroneutrality condition with [A'$_{eff}$]

$$2[V_O^{\bullet\bullet}] + [OH_O^{\bullet}] = [A'_{eff}]$$

yields a modified expression for the mass action constant:

$$K_{hydrat} = \frac{2[OH_O^g]^2}{pH_2O([A'_{eff}]-[OH_O^g])(3-[A'_{eff}]/2-[OH_O^g])}$$

The ΔH^0 and ΔS^0 values of Fig. 11 in the main paper were determined by fitting the van 't Hoff plots (employing $[A'_{eff}]$) in the range of 350-800 °C. Since the van 't Hoff plots (Fig. S9,10) have some slight deviations from perfect linearity, choosing a different *T* range for the fitting slightly changes also the ΔH^0 and ΔS^0 values. Table S3 compares the results for the 350-800 °C and 500-800 °C fitting ranges. While the high-*T* range leads to systematically more negative ΔH^0 and ΔS^0 values, the trends displayed in Fig. 11 of the main paper remain unaffected. The choice of the fitting range is always a balance; at high *T* K_{hydrat} is potentially more affected by uncertainties in the determination of the aboslute proton concentration from the dry/humid switching, while at lower *T* (high K_{hydrat}) the uncertainty in $[A'_{eff}]$ may have a stronger effect. Thus it is most important to treat all samples on a equal basis as done here.

Table S3: Comparison of ΔH^0 and ΔS^0 values obtained by different fitting ranges of the van 't Hoff plots

sample	ΔH^0 / kJ/mol	ΔS^0 / J/molK	ΔH^0 / kJ/mol	ΔS^0 / J/molK
	fitted in 350-800 °C range Fig. 11		fitted in 500-800 °C range	
SPS no Ni	-85	-94	-89	-99
SSRS 0.25wt% NiO	-88	-98	-98	-109
SSRS 0.5wt% NiO	-91	-105	-101	-116
SSRS 1wt% NiO	-88	-99	-97	-112
SPS Ni on B 0.25wt%	-94	-106	-108	-119
SPS Ni on B site 1wt%	-105	-121	-121	-138